Kerr interaction with displaced and squeezed Fock states

P. Král
Institute of Physics, Czechoslovak Academy of Sciences, Na Slovance 2, 180 40 Praha 8, Czechoslovakia
(Received 10 October 1989; revised manuscript received 22 June 1990)

Displaced and squeezed Fock states have recently been thoroughly investigated. Application of these states as the input of a Kerr nonlinear medium reveals many nonclassical effects. We solve this problem analytically and demonstrate results by numerical examples. We introduce a phase distribution for the antinormal quasidistribution $\phi_{\mathcal{A}}$ and show that the "phase" of the new states can be sharply localized at some values. This happens when revivals appear in the field. If the states are shifted by a reference wave, photon-number distributions clearly detect the structure of $\phi_{\mathcal{A}}$. Damping of the new states is briefly discussed.

I. INTRODUCTION

Considerable progress has recently been made in the production of nonclassical light states. Fields with a low level of noise become very attractive. From this point of view Fock states are the limit of noiseless states. The study of these states in various interactions has good physical reasons, since there already exist some possibilities to produce them (see also Ref. 1). In Ref. 1 we have investigated displaced and squeezed Fock states $|\beta,m\rangle_g=S(\xi)D(\beta)|m\rangle$. These states originate in a successive evolution of the Fock states $|m\rangle$ in the linear and quadratic interactions, represented by the displacement D and squeeze S operators. Squeezed Fock and squeezed thermal states have been investigated in parallel in Ref. 2, where results supplementing Ref. 1 have been found. The Fock states and their generalizations could lead to new light sources with unexpected properties without analogy in classical electromagnetic waves. These fields could be useful in such diverse areas as optical spectroscopy, communications, or biology. Further, they make possible an experimental study of the limits of quantum mechanics.

In Ref. 1 we ascertained that antinormal quasidistributions $\phi_{\mathcal{A}}$ for $|\beta,m\rangle_g$ states have the form of a modulated squeezed annulus. We have shown that various oscillations in photon-number distributions are tightly connected to the structure of $\phi_{\mathcal{A}}$. Therefore the form of $p(n)$ is to some limit predictable from $\phi_{\mathcal{A}}$. We introduced and broadly employed the one-parametric generating function for $|\beta,m\rangle_g$ states with $m>0$. The Kerr nonlinear medium, represented by the evolution operator U_3 produces crescent states.[3] These states have very low noise levels.

This paper focuses on two subjects. The first deals with new aspects of using $|\beta,m\rangle_g$ instead of coherent states in the Kerr interaction. The second concerns quantum revivals, which are characteristic for the Kerr interaction. From a physical point of view these revivals lead to states that generalize the usual coherent states to "multiphase coherent states" (MCS). They have no classical analogy, but they broaden our comprehension of the borders between quantum and classical light theory.

Interesting results, in some way similar to those found here, were also given in Refs. 4 and 5. They also make some comments on revivals for the Kerr nonlinearity. But new insight into this subject, which develops observations effected in Refs. 4 and 5, is given here. We demonstrate that fractional revivals can appear for any strength and time of evolution in the Kerr nonlinear interaction. This nonlinearity was further thoroughly examined in Ref. 6 and it was used to model nonlinear interacting oscillators in Ref. 7.

The paper is organized as follows. In Sec. II we briefly review some results for $|\beta,m\rangle_g$ states and give necessary information about the Kerr nonlinearity. In Sec. III we find the coherent-state representation $\langle\alpha|U_3|\beta,m\rangle_g$, the related antinormal quasidistribution $\phi_{\mathcal{A}}$, and some of wave functions. In Sec. IV we shift the states $U_3|\beta,m\rangle_g$ and find the antinormal characteristic function $C'_{\mathcal{A}}$ and the generating function $C_{\mathcal{N}}^{(w)'}$ for them. Further, we show how photon-number distributions $p(n)$ and factorial moments $\langle W^k\rangle_{\mathcal{N}}$ for $U_3|\beta,m\rangle_g$ with $m>0$ can be derived from $C_{\mathcal{N}}^{(w)'}$. In Sec. V we briefly mention damping of $U_3|\beta,m\rangle_g$. Section VI deals with revivals as specific features of a quantum chaos in the Kerr nonlinearity. Finally Sec. VII presents numerical results and the Conclusion touches on some experimental points of view.

II. MINIREVIEW OF DISPLACED AND SQUEEZED FOCK STATES AND THE KERR NONLINEARITY

In Ref. 1 we have defined displaced and squeezed Fock states $|\beta,m\rangle_g$ by the following formula (see also Ref. 8):

$$|\beta,m\rangle_g=S(\zeta)D(\beta)|m\rangle=S(\zeta)D(\beta)\frac{a^{\dagger m}}{\sqrt{m!}}|0\rangle\ , \tag{2.1}$$

where $D(\beta)$ and $S(\zeta)$ are a displacement and squeeze operator

$$D(\beta)=\exp(\beta a^{\dagger}-\beta^{*}a),\quad S(\zeta)=\exp(\zeta a^{\dagger 2}-\zeta^{*}a^{2})\ , \tag{2.2}$$

and $a^{\dagger},a$ are the creation and annihilation operators.

The parameters μ, ν, referred to below, are related to ζ by[8,9]

$$\zeta=(r/2)\exp(-i\theta)\ ,$$

$$\mu=\cosh(r)\ ,$$

$$\nu=\exp(-i\theta)\sinh(r)\ ,$$

and the coefficients α_0, α_0^* are defined by $\beta=\mu\alpha_0+\nu\alpha_0^*$.

In the same place we found the coherent-state representation for $|\beta,m\rangle_g$ states by the method of a generating function. We inserted the term $\exp(\lambda a^+)$ into the matrix element $\langle\alpha|\beta,0\rangle_g=\langle\alpha|\beta\rangle_g$,[9] used the Baker-Hausdorff theorem and the definition of Hermite polynomials.[10] The one-parametric representation of $\langle\alpha|\beta,m\rangle_g$ appeared in the form (see Appendix)

$$\langle\alpha|\beta,m\rangle_g=\frac{1}{\sqrt{m!}}\langle\alpha|\beta\rangle_g(\sqrt{-A}\,)^m\mathrm{H}_m\left[\frac{B}{2\sqrt{-A}}\right]\ , \tag{2.3}$$

where

$$A=\frac{\nu^*}{2\mu},\quad B=\frac{\alpha^*-\alpha_0^*}{\mu}\ .$$

The investigation of the states $|\beta,m\rangle_g$ in Ref. 1 revealed that the generating function method is a useful tool for dealing with Fock states. We damped $|\beta,m\rangle_g$ states in the one- and two-photon absorption process. The two-photon damping of a displaced and squeezed vacuum gave us a new physical insight into this damping process. Since this process damps more quickly higher intensities, the elongated ellipsis of $\phi_{\mathcal{A}}$ for a squeezed and displaced vacuum became distorted. This led to even lower noise in the states.

The Kerr medium blurs $\phi_{\mathcal{A}}$ over the space of α. If such a field is mixed with a reference beam, lower noise states could be obtained.[3] We can expect that the same mechanism could be effective for the states $|\beta,m\rangle_g$. Besides this, we will see that the blurred states can periodically pull off and give a new physical picture of the evolution in the Kerr medium.

The Hamiltonian describing this nonlinearity reads[3]

$$\hat{H}=\hbar\omega\hat{a}^\dagger\hat{a}+\hbar X(\hat{a}^\dagger)^2\hat{a}^2=\hbar\omega\hat{n}+hX\hat{n}(\hat{n}-1)\ , \tag{2.4}$$

where $\hat{n}=\hat{a}^\dagger\hat{a}$ is the number operator and X is proportional to a third-order nonlinear susceptibility χ^3. We denote the evolution operator in the interaction picture for (2.4) by $U_3(\gamma)$. For the medium of a length l and a velocity of light in the medium v, it acquires the form[3]

$$U_3(\gamma)=\exp[\tfrac{1}{2}\gamma\hat{n}(\hat{n}-1)]\ , \tag{2.5}$$

where $\gamma=2Xl/v$. Notice that this operator preserves photon-number statistics, as can be seen from (2.5). Its averaged value in the Fock state $|n\rangle$ is a periodic function of γ. Different n give various angular velocities. Superposition of these motions for a given state has physical consequences for the evolution. New coherent effects without classical analogy appear. The lack of classical analogy is probably tied to the fact that the quantum of energy $\hbar\omega$ is finite. Different Fock states have very different angular velocities and localized α-space elevations can appear. These wave packets form the revivals of the starting $\phi_{\mathcal{A}}$.

Effective investigation of these phenomena can be carried out by the following methods of calculation. The nondiagonal representation of U_3 in coherent states serves us as the starting point. It results easily[3]

$$\langle\alpha|U_3|\alpha_1\rangle=e^{-(1/2)(|\alpha|^2+|\alpha_1|^2)}\sum_{n=0}^{\infty}\frac{(\alpha^*\alpha_1)^n}{n!}e^{(i/2)\gamma n(n-1)}\ . \tag{2.6}$$

This matrix element together with the formula (2.3) enables us to gain the coherent-state representation of the field $U_3(\gamma)S(\zeta)D(\beta)|m\rangle$. It gives the antinormal quasidistributions $\phi_{\mathcal{A}}$. The Wigner quasidistribution[10] can be easily calculated, too. But it acquires both positive and negative values. There is probably no simple intuitive way to imagine such a complex field through this distribution. We will see that the antinormal quasidistribution could give us a new physical picture to the meaning of a phase for the quantum fields. As can be expected the normal quasidistribution does not exist from the same reasons as for the field $|\beta,m\rangle_g$ (see Ref. 1).

III. THE COHERENT-STATE REPRESENTATION, ANTINORMAL QUASIDISTRIBUTION, AND WAVE FUNCTIONS OF $U_3|\beta,m\rangle_g$ STATES

This section investigates antinormal quasidistributions and wave functions of the states $U_3|\beta,m\rangle_g$. The matrix elements $\langle\alpha|U_3|\beta,m\rangle_g$ contain all important information about the states $U_3|\beta,m\rangle_g$ in easily accessible form. To find $\langle\alpha|U_3|\beta,m\rangle_g$ we use the generating function of $\langle\alpha|\beta,m\rangle_g$ from the Appendix (we call it the "unwrapped" form of $\langle\alpha|\beta,m\rangle_g$).

The matrix elements $\langle\alpha|U_3|\beta,m\rangle_g$ result from the following elegant method. We insert $\langle\alpha|U_3|\alpha_1\rangle$ from (2.6) and $\langle\alpha_1|\beta,m\rangle_g$ in its "unwrapped" form into the completeness relation

$$\int|\alpha\rangle\langle\alpha|\frac{d^2\alpha}{\pi}=1 \tag{3.1}$$

and obtain

$$\langle\alpha|U_3(\gamma)S(\zeta)D(\beta)|m\rangle=\int\langle\alpha|U_3|\alpha_1\rangle\langle\alpha_1|\beta,m\rangle_g\frac{d^2\alpha_1}{\pi}$$

$$=\frac{1}{\pi}e^{-|\alpha|^2/2}\sum_{n=0}^{\infty}\frac{e^{(i/2)\gamma n(n-1)}}{n!}\alpha^{*n}\frac{\partial^n}{\partial p^n}\frac{1}{\sqrt{m!}}\frac{\partial^m}{\partial\lambda^m}$$

$$\times\int\exp\left[p\alpha_1-\frac{|\alpha_1|^2}{2}+\lambda^2A+\frac{\lambda}{\mu}(\alpha_1^*-\alpha_0^*)\right]\langle\alpha_1|\beta\rangle_g d^2\alpha_1|_{\lambda=p=0}$$

$$=\frac{1}{\sqrt{\mu m!}}\exp\left[-\frac{|\alpha|^2}{2}-\frac{|\beta|^2}{2}+\frac{\nu^*}{2\mu}\beta^2\right]$$

$$\times\sum_{n=0}^{\infty}\frac{e^{(i/2)\gamma n(n-1)}}{n!}\alpha^{*n}$$

$$\times\sum_{j=0}^{m}\binom{m}{j}(K')^j(\sqrt{-A_1})^{n+j}(\sqrt{-\mathcal{A}_2})^{m-j}\mathrm{H}_{n+j}\left[\frac{B_1}{2\sqrt{-A_1}}\right]\mathrm{H}_{m-j}\left[\frac{B_2-B_1K'}{2\sqrt{-\mathcal{A}_2}}\right], \tag{3.2}$$

where the coefficients are

$$A_1=\frac{-\nu}{2\mu},\quad A_2=A,\quad A_3=\frac{1}{\mu},\quad B_1=\frac{\beta}{\mu},\quad B_2=\frac{-\alpha_0^*}{\mu},\quad K'=\frac{A_3}{2A_1},\quad \mathcal{A}_2=A_2-\frac{A_3^2}{4A_1}. \tag{3.3}$$

In (3.2) we have replaced α_1^n by $(\partial^n/\partial p^n)\exp(p\alpha_1)|_{p=0}$. Also we used the matrix element $\langle\alpha|\beta\rangle_g$ from Ref. 9 and performed the integration with the help of the following integral:[11]

$$\int\exp[-B|\beta|^2+(C/2)\beta^{*2}+(C_1/2)\beta^2+D_1\beta+D\beta^*]d^2\beta=\frac{\pi}{\sqrt{K}}\exp\left[\frac{1}{K}[DD_1B+D^2(C_1/2)+D_1^2(C/2)]\right],$$

$$K=B^2-CC_1,\quad \mathrm{Re}K>0,\quad \mathrm{Re}[B+(C_1+C)/2]>0. \tag{3.4}$$

Finally we transformed p, λ to other coefficients by the linear transformation $(\rho'=\lambda,\rho=p+K'\lambda)$, because they appeared after the integration in a common product. The Hermite polynominals resulted in the way shown in the Appendix.

The formula (3.2) reveals how the elements $\langle\alpha|\beta,m\rangle_g$ are superimposed. This information could be useful in physical deliberations. Another rearrangement simplifies (3.2)

$$\langle\alpha|U_3|\beta,m\rangle_g=e^{-|\alpha|^2/2}\sum_{n=0}^{\infty}\alpha^{*n}f(n)$$

$$=e^{-|\alpha|^2/2}\sum_{n=0}^{\infty}f(n)\frac{\partial^n}{\partial p^n}e^{p\alpha^*}\Big|_{p=0}. \tag{3.5}$$

The form of $f(n)$ is obvious from its definition in (3.5), if the last is compared with (3.2). Notice that the parameter α appears in the last expression of (3.5) only in the argument of the exponential function. This greatly simplifies integrations performed below.

Our next goal is the antinormal quasidistributions $\phi_{\mathcal{A}}$ (Ref. 10) for the states $U_3|\beta,m\rangle_g$. This is the main result, which will answer basic questions about the problem. We postpone them to Sec. VII. $\phi_{\mathcal{A}}$ can be introduced in the following form:

$$\phi_{\mathcal{A}}(\alpha)=\frac{1}{\pi}\langle\alpha|\hat{\rho}|\alpha\rangle$$

$$=\frac{1}{\pi}|\langle\alpha|U_3|\beta,m\rangle_g|^2$$

$$=\frac{e^{-|\alpha|^2}}{\pi}Le^{p_1\alpha^*+p_2\alpha}$$

$$=\frac{e^{-|\alpha|^2}}{\pi}\sum_{n,n'=0}^{\infty}f(n)f^*(n')\alpha^{*n}\alpha^{n'}, \tag{3.6}$$

where $\hat{\rho}$ is the density operator and L follows:

$$L=\sum_{n,n'=0}^{\infty}f(n)f^*(n')\frac{\partial^n}{\partial p_1^n}\frac{\partial n'}{\partial p_2^{n'}}\Big|_{p_1=p_2=0}. \tag{3.7}$$

The expression with L in (3.6) is in fact a two-parametric representation of $\phi_{\mathcal{A}}$, described in Ref. 1. If we substitute $\alpha=\alpha-a_0$ in (3.6), we obtain $\phi_{\mathcal{A}'}$ for the shifted states $D(a_0)U_3|\beta m\rangle_g$, which could arise from the superposition of $U_3|\beta,m\rangle_g$ with a strong reference beam.[3] Results in Sec. IV will be presented for this generalized $\phi_{\mathcal{A}'}$.

Now consider the following wave functions $\langle q|U_3|\beta,m\rangle_g$. They are the coordinate representation of the fields $U_3|\beta,m\rangle_g$. They can be found similarly as $\langle q|\beta,m\rangle_g$ in Ref. 1. We make use of (3.5), $\langle q|\alpha\rangle$ from Ref. 12, the completeness relation (3.1), and as a result obtain

$$\langle q|U_3|\beta,m\rangle_g=\left[\frac{\omega}{\pi\hbar}\right]^{1/4}e^{-Q^2/2}\sum_{n=0}^{\infty}f(n)\left[\frac{\partial}{\partial p}\right]^n\int\exp(-|\alpha|^2-\tfrac{1}{2}\alpha^2+p\alpha^*+\sqrt{2}\alpha Q)\frac{d^2\alpha}{\pi}$$
$$=\left[\frac{\omega}{\pi\hbar}\right]^{1/4}e^{-Q^2/2}\sum_{n=0}^{\infty}f(n)\mathrm{H}_n(Q)2^{-n/2}\,, \tag{3.8}$$

where $Q=q\sqrt{\omega/\hbar}$. The integration procedure, was accomplished as in (3.2). The wave functions (3.8) are demonstrated by selected numerical examples in Sec. VII. They arise by a coherent projection of $\phi_{\mathcal{A}}$ on one coordinate axis. This results in many interference oscillations for longer times of evolution in the Kerr medium. The p representation and other wave functions of the fields can be found analogously.

Wave functions and coordinate variances were investigated in Ref. 5 for a damped and amplified nonlinear oscillator. Some of the revival effects can be observed there. Now we will examine the scalar product of $U_3(\gamma)|\beta,m\rangle_g$ with $U_3(\gamma')|\beta',m'\rangle_g$. It represents the overlapping of the two wave functions. Physically, the second power of its modulus gives the probability of finding the oscillator in the state $U_3(\gamma')|\beta',m'\rangle_{g'}$, if we know that it is in the state $U_3(\gamma)|\beta,m\rangle_g$. Originally the Fock states were orthogonal $\langle m|m'\rangle=\delta_{mm'}$, but in the course of evolution this relation breaks down. Intuitively we can expect that the overlapping of two states $U_3(\gamma)|\beta,m\rangle_g$ with different parameters is nonzero, if the corresponding $\phi_{\mathcal{A}},\phi'_{\mathcal{A}}$ overlap in the plane α. We can find the scalar product similarly as we have found ${}_{g'}\langle\beta_2,m_2|\beta_1,m_1\rangle_g$ in Ref. 1. After a simple algebra, there results

$${}_{g'}\langle\beta',m'|U_3'^{\dagger}U_3|\beta,m\rangle_g$$
$$=L_{12}\int\exp(-|\alpha|^2+p_1\alpha^*+p_2\alpha)\frac{d^2\alpha}{\pi}$$
$$=L_{12}\exp(p_2p_1)\,. \tag{3.9}$$

Here (3.4) and (3.5) were used and L_{12} is a slightly changed operator L from (3.7). In its definition it is necessary to substitute

$$f(n)=f_1(n),\quad f^*(n')=f_2^*(n')\,. \tag{3.10}$$

The indices 1,2 at f in (3.10) correspond to the two states in (3.9). If we convert the product p_2p_1 in (3.9) into another one, as in (3.2), this expression can be rearranged. To this purpose we make the transformation toward the new parameters

$$p_1=\rho_1+\rho_2,\quad p_2=\rho_1-\rho_2\,, \tag{3.11}$$

which permits us to rewrite the term with the partial derivatives in L_{12}. The explicit form of (3.9) easily appears:

$${}_{g'}\langle\beta',m'|U_3'^{\dagger}U_3|\beta,m\rangle_g=\sum_{n,n'=0}^{\infty}f_1(n)f_2^*(n')\frac{1}{2^{n+n'}}\sum_{k=0}^{n}\sum_{l=0}^{n'}\binom{n}{k}\binom{n'}{l}(-1)^{n'-l}i^{k+l}\mathrm{H}_{k+l}(0)\mathrm{H}_{n+n'-k-l}(0)\,. \tag{3.12}$$

Here the following property of Hermite polynomials:[13]

$$\mathrm{H}_{2n}(0)=(-1)^n\frac{(2n)!}{n!},\quad \mathrm{H}_{2n+1}(0)=0\,, \tag{3.13}$$

can be used to simplify (3.12). The structure of (3.12) has a general form, which will often appear in the subsequent analysis. It is of interest that if $\phi_{\mathcal{A}}$ from (3.6) interacts linearly with another quantum mode, the new $\phi_{\mathcal{A}}$ acquires a form similar to (3.12). Physical consequences of this interaction on revival states (see below) are nontrivial. These investigations are planned to be published later by some of our colleagues.

IV. GENERATING FUNCTIONS, PHOTON-NUMBER DISTRIBUTIONS, AND FACTORIAL MOMENTS FOR $U_3|\beta,m\rangle_g$ STATES

So far we have examined wave functions of the fields $U_3(\gamma)|\beta,m\rangle_g$ in the coherent states and the coordinate representations. We can continue our investigation with the moments of the type $\langle a^{\dagger i}a^j\rangle$, $\langle a^i a^{\dagger j}\rangle$ for equal and unequal i,j. They can be combined to give photon-number distributions $p(n)$ or factorial moments $\langle W^k\rangle_{\mathcal{N}}$.[10] The starting point will be the antinormal quasidistribution $\phi_{\mathcal{A}}$ from the preceding section.

The Fourier transform of $\phi_{\mathcal{A}}$ from (3.6) gives the antinormal characteristic function $C_{\mathcal{A}}$ (Ref. 10)

$$C_{\mathcal{A}}(\xi)=\int\phi_{\mathcal{A}}(\alpha)\exp(\xi\alpha^*-\xi^*\alpha)d^2\alpha$$
$$=L\exp[(p_1+\xi)(p_2-\xi^*)]\,, \tag{4.1}$$

where (3.4) and L from (3.7) have been used. Together with the normal characteristic function $C_{\mathcal{N}}$ (Ref. 10) they generate the above shown moments for generally different i,j.

If we put a Kerr medium in an interferometer,[3] we could produce the field $D(a_0)U_3|\beta,m\rangle_g$. This state can have sub-Poissonian distributions $p(n)$, which can be detected as photon antibunching in the Hanbury Brown-Twiss experiment. $C'_{\mathcal{A}}$ for this field can be found as follows. We make the shift $\alpha=\alpha-a_0$ in $\phi_{\mathcal{A}}$ from (4.1) and obtain

$$C'_{\mathcal{A}}(\xi)=C_{\mathcal{A}}(\xi)\exp(a_0^*\xi-a_0\xi^*)\,. \tag{4.2}$$

Here $C_{\mathcal{A}}$ from (4.1) is multiplied by a factor resulting from the shift. We should show the explicit form of (4.2). After a transformation analogous to (3.11) $C'_{\mathcal{A}}$ acquires the form of (3.12) with f, f^* in place of f_1, f_2^*. The arguments of the first and second Hermite polynomial and the exponential prefactor in (3.12) are now

$$-i\frac{\xi-\xi^*}{2},\quad -\frac{\xi+\xi^*}{2};\quad \exp(a_0^*\xi-a_0\xi^*-|\xi|^2)\ . \tag{4.3}$$

At this point we will stop our investigation of $C_{\mathcal{A}}, C'_{\mathcal{A}}$ because of the lack of space. But we encourage the interested reader to do this at least for a few small moments. Despite its complexity the formula (3.12) and moments derived from it can be rather easily summed by a computer.

In the rest of this section we can calculate the photon-number generating functions $C_{\mathcal{N}}^{(w)}$ and $C_{\mathcal{N}}^{(w)'}$.[10] They easily result from their definitions

$$C_{\mathcal{N}}^{(w)}(\lambda)=\frac{1}{\pi\lambda}\int \exp\left[-\frac{|\xi|^2}{\lambda}\right]C_{\mathcal{N}}(\xi)d^2\xi$$

$$=L\exp[p_1p_2(1-\lambda)]\ , \tag{4.4}$$

$$C_{\mathcal{N}}^{(w)'}=C_{\mathcal{N}}^{(w)}\exp[-\lambda(|a_0|^2+a_0p_2+a_0^*p_1)]\ . \tag{4.5}$$

Here $C_{\mathcal{N}}$ is the normal characteristic function, related to $C_{\mathcal{A}}$ by[10]

$$C_{\mathcal{N}}(\xi)=C_{\mathcal{A}}(\xi)\exp(|\xi|^2)\ .$$

As before, we yet present the explicit form of (4.5). Two transformations must be performed to attain this goal. The first reads

$$p_1'=p_1+c_1,\quad p_2'=p_2+c_2\ ,$$

where c_1, c_2 are defined in (4.7). The second is the same as in (3.11). After a little algebra we obtain $C_{\mathcal{N}}^{(w)'}$ in the form of $C'_{\mathcal{A}}$. But in $C_{\mathcal{N}}^{(w)'}$ still the term $(\sqrt{A}\,)^{n+n'}$ appears in the product with Hermite polynomials. The new arguments and prefactor follow:

$$-i\sqrt{A}\,\frac{c_1+c_2}{2},\quad -\sqrt{A}\,\frac{c_1-c_2}{2};\quad \exp(-\lambda|a_0|^2)\ , \tag{4.6}$$

where the coefficients are

$$A=1-\lambda,\quad c_1=\frac{-\lambda}{1-\lambda}a_0,\quad c_2=c_1^*\ . \tag{4.7}$$

A similar comment can be given to the photon-number generating function $C_{\mathcal{N}}^{(w)}$ and $C_{\mathcal{N}}^{(w)'}$ as for $C_{\mathcal{A}}, C'_{\mathcal{A}}$. In principle they enable us to gain factorial moments $\langle W^k\rangle_{\mathcal{N}}$ and photon-number distributions $p(n)$ by[10]

$$\langle W^k\rangle_{\mathcal{N}}=(-1)^k\frac{d^k}{d\lambda^k}C_{\mathcal{N}}^{(w)}(\lambda)\bigg|_{\lambda=0}\ , \tag{4.8}$$

$$p(n)=\frac{(-1)^n}{n!}\frac{d^n}{d\lambda^n}C_{\mathcal{N}}^{(w)}(\lambda)\bigg|_{\lambda=1}\ . \tag{4.9}$$

In the general case $a_0=0$ no closed formulas for $p(n)$ and $\langle W^k\rangle_{\mathcal{N}}$ exist. But for small k and n the generating function $C_{\mathcal{N}}^{(w)'}$ can be successively differentiated in (4.8) and (4.9). For the simple case $a_0=0$ the Hermite polynomials need not be differentiated [their arguments are 0 in (4.6)], so that closed formulas can easily be found. But photon-number statistics and factorial moments for $U_3|\beta,m\rangle_g$ states are the same as for the field $|\beta,m\rangle_g$. In Sec. VII we show some of the photon-number distributions for the states $D(a_0)U_3|\beta,m\rangle_g$, calculated by another method. There we will see how the reference beam[3] clearly discloses the hidden structure in $\phi_{\mathcal{A}}$.

Production of states $D(a_0)U_3|\beta,m\rangle_g$ in the Kerr interferometer might be a great problem in practice. The presence of various sources of a noise may cover the structure in $\phi_{\mathcal{A}}$. Since the noise in the field grows with the time of interaction, stronger nonlinearities could help solve the problem. On the other hand, low-temperature experiments can substantially diminish the noise of a scattering system.

V. DAMPING OF $U_3|\beta,m\rangle_g$ STATES

In this section we briefly summarize results obtained for damped $D(a_0)U_3(\gamma)|\beta,m\rangle_g$ states. When damping is included into the nonlinear oscillator model (2.4), both the result and the method of the solution become very difficult. This problem was solved in Ref. 5 with $\phi_{\mathcal{A}}$ for a coherent state and in Ref. 6 for an arbitrary $\phi_{\mathcal{A}}$. Despite the fact that this investigation is very realistic because of a noise production in the Kerr interaction process, here we choose a simpler approximation. We concentrate on the problem of damping of $\phi_{\mathcal{A}}$ for $U_3|\beta,m\rangle_g$ states, prepared in the nonlinear Kerr oscillator.

We present analytical results for damped antinormal quasidistributions $\phi'_{\mathcal{A}}$, characteristic functions $C'_{\mathcal{A}}$, and generating functions $C_{\mathcal{N}}^{(w)'}$.

The Green function in the interaction picture for a one-mode damping process reads[12]

$$G(\alpha,\alpha_1)=\frac{1}{\pi C}\exp\left[-\frac{1}{C}|\alpha-\alpha_1e^{-(\gamma'/2)t}|^2\right]\ , \tag{5.1}$$

where

$$C=(\bar{n}+1)(1-e^{-\gamma' t})\ , \tag{5.2}$$

and $\bar{n}$ and γ' are the mean number of chaotic phonons and damping rate. We shift $\phi_{\mathcal{A}}$ from (3.6) and insert this $\phi'_{\mathcal{A}}$ into the convolution relation for a damped solution. We also use (3.4) and as a result obtain the damped antinormal quasidistribution $\phi'_{\mathcal{A}}$

$$\phi'_{\mathcal{A}}(\alpha,t)=\int\phi'_{\mathcal{A}}(\alpha_1)G(\alpha,\alpha_1)d^2\alpha_1$$

$$=\frac{A}{\pi C}\exp\left[-|a_0|^2-\frac{|\alpha|^2}{C}\right]$$

$$\times L\exp[A(\lambda_1+D)(\lambda_2+D^*)-\lambda_1a_0^*-\lambda_2a_0]\ , \tag{5.3}$$

where the parameters A, D are

$$A=\frac{C}{C+e^{-\gamma' t}},\quad D=a_0+\frac{\alpha}{C}e^{-(\gamma'/2)t};$$
$$c_1=\frac{AD-a_0}{A},\quad c_2=c_1^{*}\ . \tag{5.4a}$$

$\phi'_{\mathcal{A}}$ from (5.3) can be rearranged to the form of $C_{\mathcal{N}}^{(w)'}$ from the preceding section. We must substitute A,c_1,c_2 from (4.7) by the expressions from (5.4a) and replace the exponential prefactor in (4.6) by

$$\frac{A}{\pi C}\exp\left[-|a_0|^2-\frac{|\alpha|^2}{C}+A|D|^2\right]. \tag{5.4b}$$

The damped $C'_{\mathcal{A}}$ results similarly. Using the definition of $C_{\mathcal{A}}$ from (4.1) and $\phi'_{\mathcal{A}}$ from (5.3), $C'_{\mathcal{A}}$ acquires the previous form of $C_{\mathcal{N}}^{(w)'}$. The new coefficients A',c_1,c_2 and prefactor, analogous to (5.4b), are

$$A'=G+A,$$
$$c_1=\frac{1}{A'}[GB_1+a_0(A-1)]\ , \tag{5.5a}$$
$$c_2=\frac{1}{A'}[GB_2+a_0^{*}(A-1)]\ ,$$

and

$$\exp[GB_1B_2+|a_0|^2(A-1)]/[B(C+e^{-\gamma' t})]\ . \tag{5.5b}$$

The unknown parameters follow:

$$G=Be^{-\gamma' t},\quad B_1=a_0+\frac{\xi}{B}e^{\gamma' t/2}\ ,$$
$$B_2=a_0^{*}-\frac{\xi^{*}}{B}e^{\gamma' t/2},\quad B=\frac{A}{C}\ ,$$

and A,C are the same as in (5.4a).

Finally the bilinear form in λ_1,λ_2 also remains in the exponent of the damped generating function $C_{\mathcal{N}}^{(w)'}$, which acquires the form of the undamped $C_{\mathcal{N}}^{(w)'}$. Making use of the definition (4.4) the result easily appears. The new coefficients A',C_1,C_2 and the prefactor read

$$A'=G+A-\frac{e^{-\gamma' t}}{B'},\quad c_1=a_0\left[1-\frac{1}{A'}\right],\quad c_2=c_1^{*}\ , \tag{5.6a}$$

$$\exp[|a_0|^2(A'-1)]/[\lambda BB'(C+e^{-\gamma' t})]\ , \tag{5.6b}$$

where $B'=(1/B)+(1/\lambda)-1$ and A,B,C,G are the same as in (5.5).

The damped $C_{\mathcal{N}}^{(w)'}$ gives the damped photon-number distributions $p(n)$ and factorial moments $\langle W^k\rangle_{\mathcal{N}}$ from (4.8) and (4.9) in the same way as $C_{\mathcal{N}}^{(w)'}$ with coefficients in (4.6) and (4.7).

We would still like to call attention to the fact that all functions $(\phi'_{\mathcal{A}},C'_{\mathcal{A}},C_{\mathcal{N}}^{(w)'})$ calculated in this section were exponential functions and that in their arguments the parameters λ_1,λ_2 appeared exactly in the second power. This is connected with the bilinear structure of the antinormal quasidistribution $\phi_{\mathcal{A}}$ (the diagonal coherent-state representation of the density matrix). It was the principal point of the success of our analysis. Each of two wave functions in the density matrix produces one of the coefficients λ_1,λ_2. It is very interesting how these coefficients transform to the damped density matrix, which already cannot be resolved onto two wave functions. Without using the methods of parameters, there would be little chance of finding analytical results for the damped states $D(a_0)U_3(\gamma)|\beta,m\rangle_g$.

VI. REVIVALS IN THE KERR INTERACTION

Much effort was devoted to invent various wave packets since the time of Schrödinger. Generally, this meant trying to find new states that even more resembled objects like a photon or a particle. These states were the building blocks of quantum mechanics. We will try to show in this section another kind of state lying on the boundary between classical and quantum mechanics. These states even more call to mind the concept of a particle.

Revivals in $\phi_{\mathcal{A}}$ are closely related to the structure of the matrix element $\langle\alpha|U_3|\alpha_1\rangle$ in (2.6). Notice that the argument of the exponential function in the sum acquires the form $(i\gamma/2)n(n-1)$. This suggests that the quasidistribution $\phi_{\mathcal{A}}$ completely returns to its starting shape, if $\gamma/2=2\pi$. The fact that revivals can also be observed for $\gamma=\pi$ was already noted in Ref. 4 and in other papers[14] it was further examined. Quite recently Ref. 15 appeared, which could help to classify phenomena observed by us. Now we will try to explain how revival structures in $\phi_{\mathcal{A}}$ can arise, generalizing those described in Refs. 4 and 14.

The sum of the arithmetic series of the first natural numbers $1,2,3,\cdots,n$ is $S=n(n+1)/2$. The last expression appears in the exponent of (2.6), but with n substituted by $n-1$. If the variable γ is of the form $2\pi/k$, where k is a natural number, the resulting exponent in (2.6) would be $(i2\pi/k)n(n-1)/2$. The difference between this term and the following one $(i2\pi/k)(n+1)n/2$ is $(i2\pi/k)n$. So that varying n in the set of natural numbers, the exponent acquires only the values $(i2\pi/k,i4\pi/k,\ldots,i2\pi)$, neglecting a coefficient equal to a multiple of 2π. Now we set $\gamma=2\pi/k$ and observe the remaining terms $(\alpha^{*}\alpha_1)^n$ in (2.6). If the phase of $\alpha^{*}\alpha_1$ gains one of the shown k values, the phase of its nth power again falls into the above-mentioned set. This leads to a constructive interference of the terms in the sum (2.6) and results in a local elevation of $\phi_{\mathcal{A}}$. If the phase of $\alpha^{*}\alpha_1$ is very different from one of the shown values, terms in the series (2.6) have accidental phases, densely placed in the interval $(0,2\pi)$. As a consequence a local elevation in $\phi_{\mathcal{A}}$ does not appear. Accidental phases of terms in (2.6) even come if $\gamma\neq 2\pi/k$. $\alpha^{*}\alpha_1$ may then be arbitrary. As a result only accidental elevations appear in $\phi_{\mathcal{A}}$.

We might expect that, if $\gamma=2\pi/k$, then k phases of α should exist, at which $\phi_{\mathcal{A}}$ looks the same way. We will see examples of this in the next section. For $\gamma=2\pi/k$ the starting pattern of $\phi_{\mathcal{A}}$ will reappear k times on the circle centered above the center of the coordinate system. The radius of this circle is equal to the starting shift of $\phi_{\mathcal{A}}$. These new objects are placed there regularly with the angle $2\pi/k$ between neighbors. The parameter γ,

which is equal to the product of the interaction constant and time, acquires these important values $2\pi/k$ ($k=1,2,3,\ldots$) in every neighborhood of zero. Therefore interference effects might appear for times as small as we want. An important exception to this rule comes if the dimension of the starting pattern of $\phi_{\mathcal{A}}$ is larger than some limit, which depends on the radius of the circle on which $\phi_{\mathcal{A}}$ lies. Then the new k objects will not have places on the circle, and an interference diminishes them. We may say that for $2\pi|\alpha_0|k > d$, where d is the "dimension" of the starting $\phi_{\mathcal{A}}$ and α_0 the coherent shift connected with β (see Sec. II), the new objects are revealed and for the reversed inequality they are hidden due to the interference. This is in accord with reality, where for small γ and α_0 we do not observe such revivals. We need greater γ or α_0 to see them.

To conclude this section we note that revivals, similar to those discovered here, were observed in Ref. 15 for an atomic system. They were generally analyzed there and called fractional revivals. This is yet another result of the rapidly developing field of fractal physics. Probably the fractal structure of time evolutions in quantum mechanics could be more easily realizable than it is in classical physics.

VII. NUMERICAL RESULTS

In the section (i) below we show examples of charts for antinormal quasidistributions $\phi_{\mathcal{A}}$ after the Eq. (3.6). In (ii) we introduce intuitive phase distributions for the antinormal quasidistributions $\phi_{\mathcal{A}}$. We show how the phase can be sharply quantized to some periodic values in the limit of a strong field. In (iii) we will present the coordinate wave functions (3.8) by a few examples. Finally in the section (iv) we present photon-number distributions for some of $\phi_{\mathcal{A}}$ from (i), which are yet shifted.

(i) In this section $\phi_{\mathcal{A}}$ from (3.6) are calculated for the maximum number of terms in the sum $n_{\max}=65$. This implies that the results are without serious errors at most for $|\alpha|=5-6$. Nevertheless, some maps are presented with $|\alpha_{\max}|=7$ for orientation in the marginal parts of $\phi_{\mathcal{A}}$. In the following figures the plane α has the center of the coordinate system in the center of the lined place. The real axis goes along the lines and the imaginary axis lies parallel to the line-end boundary. The basis is a square with the half length of base d.

In Fig. 1 we can see the evolution of the shifted Fock states with $m=2$, $\alpha_0=3.5$, $\nu=0.08$ ($\cong 0$), $d=7$, and $\gamma=0,0.5,0.15,0.25$ for the cases (a)–(d). The coordinate center is outside the ringlike $\phi_{\mathcal{A}}$. We observe that the ring breaks into a series of disconnected hills, in the same way as in Ref. 1 under a pure squeezing. The difference is that now the elevations are not in a line, but lie on something, which reminds us of an Archimedes spiral. When the distribution blurs around the coordinate center a phase uncertainty grows in the field. Each peak corresponds to a phase-localized wave packet. But peaks with the same shape and a different distance from the coordinate center have different meaning. They pertain to a nonequal number of Bose particles. We can say that this number is $|\alpha_0|^2$ times the probability in the given peak.

Figure 2 presents $\phi_{\mathcal{A}}$ as in Fig. 1 but for parameters $m=5$, $\alpha_0=1.5$, $\nu=0.08$, $d=5$. The values $\gamma=0.15,0.35,1,2\pi/3$ correspond to cases (a)–(d). Here the coordinate center lies inside the ringlike $\phi_{\mathcal{A}}$. As a result $\phi_{\mathcal{A}}$ resembles chaotically moving wave packets, especially for great γ in (c). When revivals appear the struc-

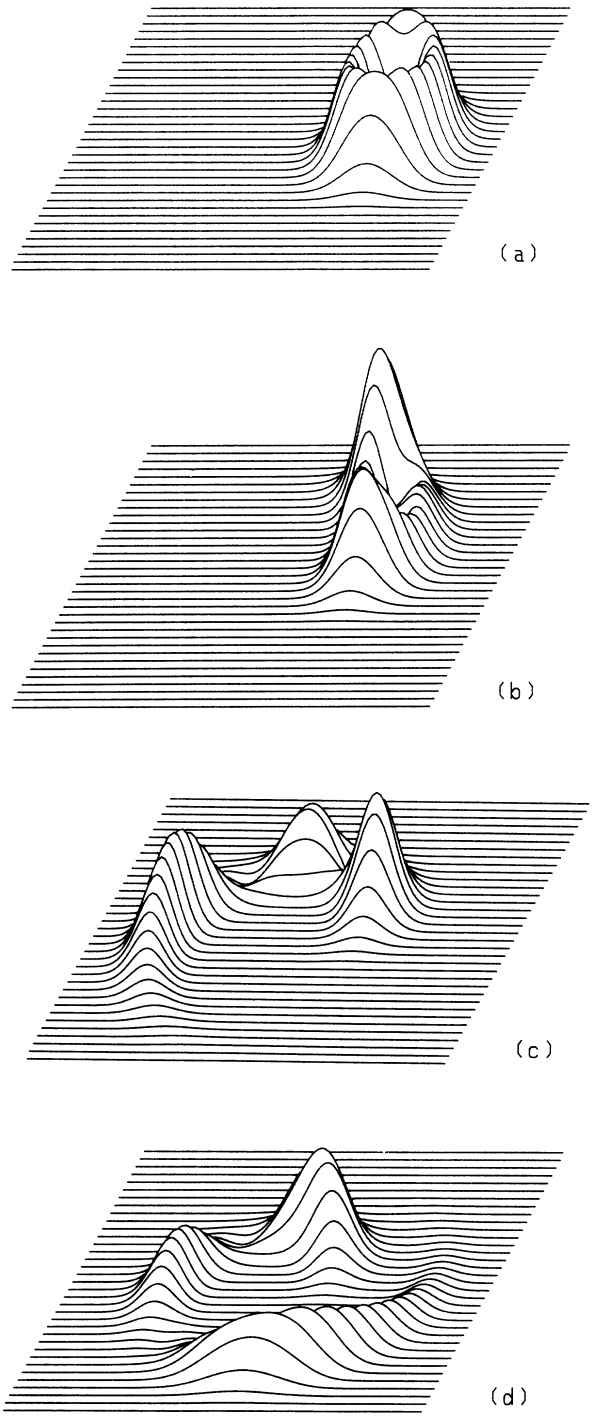

FIG. 1. Evolution of the antinormal quasidistribution $\phi_{\mathcal{A}}$ for the state $U_3|\beta,m\rangle_g$, with parameters $m=2$, $\alpha_0=3.5$, $\nu=0.08$, and $d=7$. Cases (a)–(d) correspond to $\gamma=0,0.05,0.15,0.25$.

ture of $\phi_{\mathcal{A}}$ evolves into symmetric, but unpredictable forms. The case (d) shows quantum revivals for $\gamma=2\pi/3$. Different parts of $\phi_{\mathcal{A}}$ interfere and $\phi_{\mathcal{A}}$ does not resemble the starting ringlike shape. The motion of regions with accidental phase and probability magnitude can be observed on phase-dependent moments (moments shown in the beginning of Sec. IV with $i\neq j$).

Figure 3 demonstrates the behavior of $\phi_{\mathcal{A}}$ for the squeezed Fock state with large $m=10$ and $\alpha_0=0.2$, ($\cong 0$), $\nu=0.5$, $d=7$, with $\gamma=0,0.05,0.15,\pi$, for cases (a)–(d). We observe that the ends of the elliptical $\phi_{\mathcal{A}}$ start to rotate around the center. Later many oscillating regions appear in the middle part of $\phi_{\mathcal{A}}$. Lower ends of $\phi_{\mathcal{A}}$ can be seen in (c). In Fig. 3(d) coherence in the field leads to the revealing of three parts in $\phi_{\mathcal{A}}$. They represent three packets with different phases and comparable number of particles.

We will show what is common to all these figures. In each of them there exist some points or axes of symmetry. The case (a) has a center of symmetry and two axes

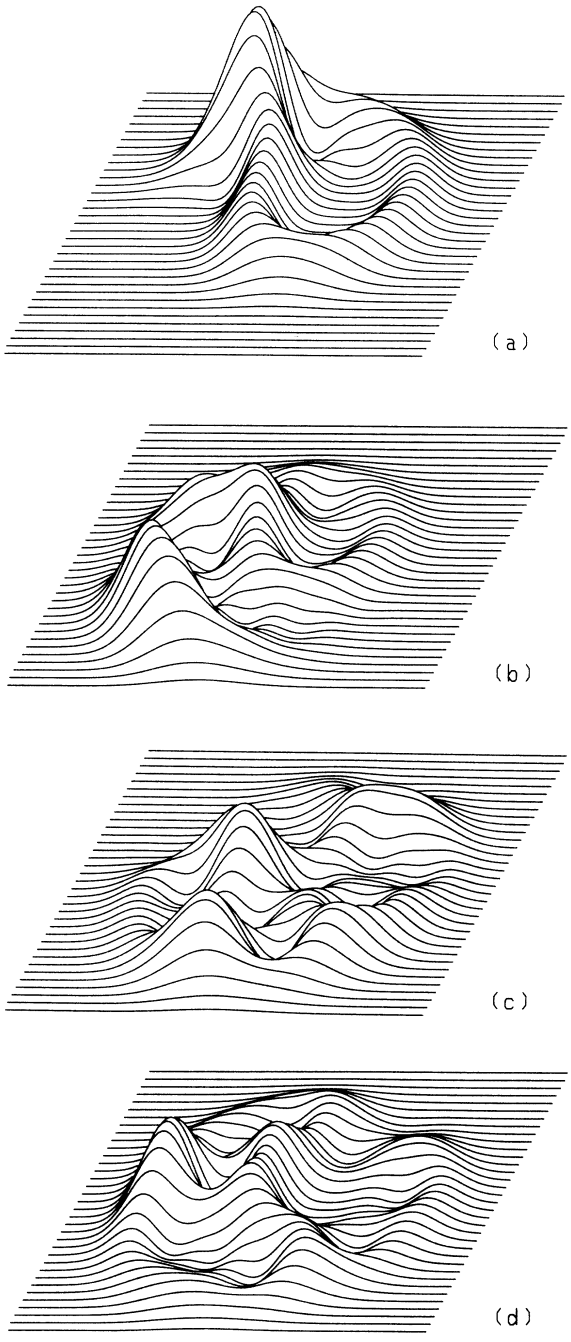

FIG. 2. The same as in Fig. 1, but for coefficients $m=5$, $\alpha=1.5$, $\gamma=0.08$, and $d=5$. Cases (a)–(d) belong to $\gamma=0.15,0.35,1,2\pi/3$, respectively.

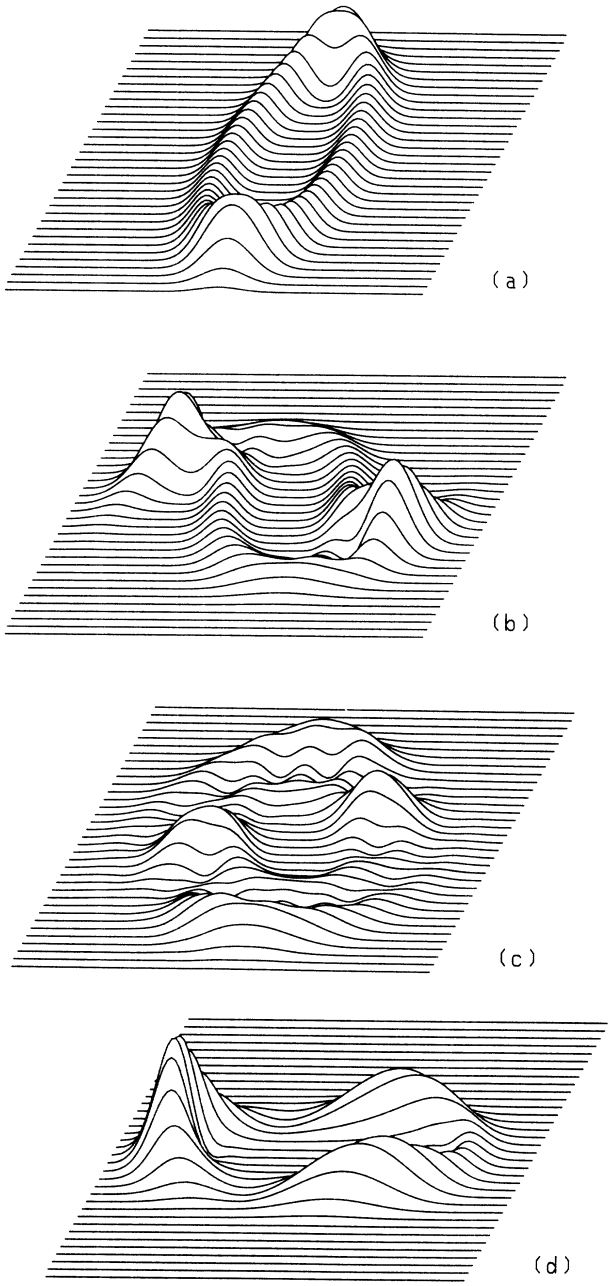

FIG. 3. As in Fig. 1 with parameters $m=10$, $\alpha_0=0.2$, $\gamma=0.5$, and $d=7$. Surfaces (a)–(d) have $\gamma=0,0.05,0.15,\pi$.

of symmetry. Cases (b) and (c) have only the center of symmetry. The case (d) gains a new axis of symmetry. Therefore in all these examples the average intensity $\langle E \rangle$ is zero, but the moment $\langle E^2 \rangle$ can be large. The fields have such phase distributions, which ensure $\langle E \rangle = 0$.

The "multiphase coherent states" (see comment to Fig. 8) can induce "multiphase responses" in systems. This can substantially change the dynamic, if it depends on the phase of the field. Every wave packet from the field produces its own action on the system. Because these packets are coherently connected the system could undergo an unexpected evolution. It would be possible to study a dynamic in different "phase channels" of the system and a correlation of channels. We must keep in mind that wave packets which we discuss here are something completely different from what we usually imagine in space. They correspond to a one-mode field. For example, an optical pulse is a superposition of many monochromatic waves in coherent states. If we produce such a pulse from the "multiphase coherent state," we obtain an optical pulse for which $\langle E \rangle = 0$ holds in all the space. Then the moment $\langle E^2 \rangle$ will determine the shape of the pulse.

In Fig. 4 is plotted the evolution of a squeezed Fock state with the parameters $m = 4$, $\alpha_0 = 0.05$, $(=0)$, $\nu = 1$, $d = 7$, and $\gamma = 0, 0.05, 0.15, 0.25$ for the cases (a)–(d), respectively. Now the original row of hills deforms itself into a form similar to a "spiral galaxy," which continuously increases the angle of rotation of its broken arms. For a large γ the galaxy structure disappears in quick interference oscillations. Now the field is nearly phase independent, as for the Fock state. But the phase coherence did not disappear from the mode. It became hidden and its presence can be seen in Figs. 4(e) and 4(f). They are the continuation of cases (a)–(d) for $\gamma = \pi$ and $2\pi/3$. The phase in Fig. 4(e) is localized to one value, but the amplitude becomes nonzero around more values. This will be even better seen on the wave function below. Yet another interesting comment could be given to Fig. 4(e). While in cases (a)–(d) the average intensity is zero $\langle E \rangle = 0$, this is not true in case (e), which presents revivals with $n = 2$. We can expect that some "symmetry-breaking" process arose during the evolution. Later we will try to show that it can be active if we are interested in the nth revival of $\phi_{\mathcal{A}}$ and this $\phi_{\mathcal{A}}$ cannot be placed n

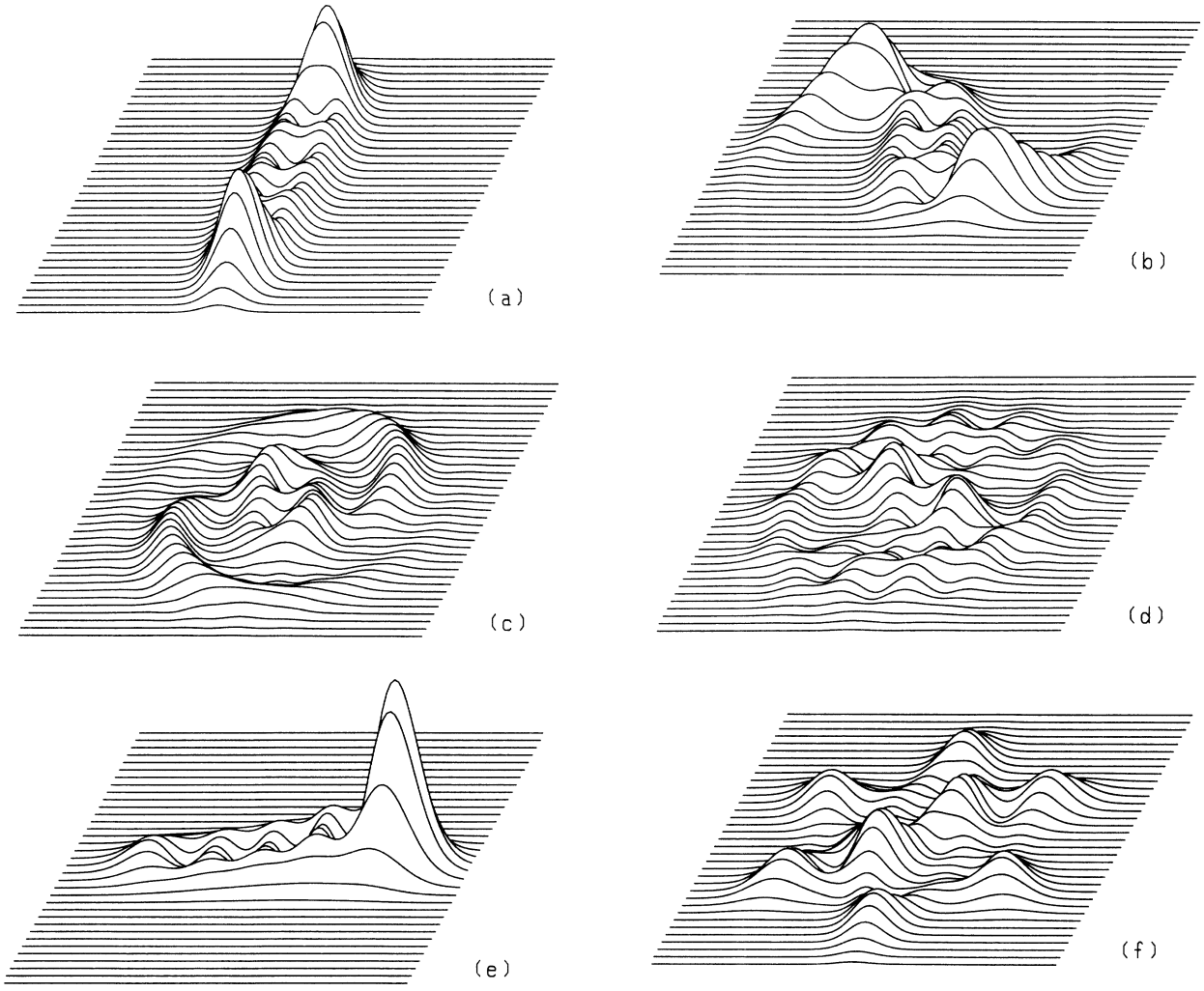

FIG. 4. As in Fig. 1 but $m = 4$, $\alpha_0 = 0.05$, $\gamma = 1$, and $d = 7$. Cases (a)–(f) correspond to $\gamma = 0, 0.05, 0.15, 0.25, \pi, 2\pi/3$.

times in the plane α. The calculation of $\langle E \rangle$ certainly would be very interesting. It can be performed on the basis of the results (4.3), (3.12). Revivals renew the initial $\phi_{\mathcal{A}}$ in Fig. 4(f) in a very suggestive way. Symmetry of the field is lower here, but the phase is localized to six similar maxima.

Figure 5 is reminiscent of the previous one, but the shift is $\alpha_0=2$ and $d=7$. The values of $\gamma=0.05,0.15,0.25$ correspond to cases (a)–(c). Here it can be seen how one of the two arms breaks down into a lot of separated hillocks. This is a consequence of the central asymmetry ($\alpha_0\neq 0$) and the resulting shift of one of the arms toward higher α. In Fig. 5(d) we changed $\nu=0.8$, $\gamma=\pi$ and $|\alpha_0|=2.5$ for a better view. In addition, the phase of α_0 is for the first time nonzero, $\varphi=0.7$. Figure 5(d) reconstructs the starting "canoelike" $\phi_{\mathcal{A}}$ in two exemplars.

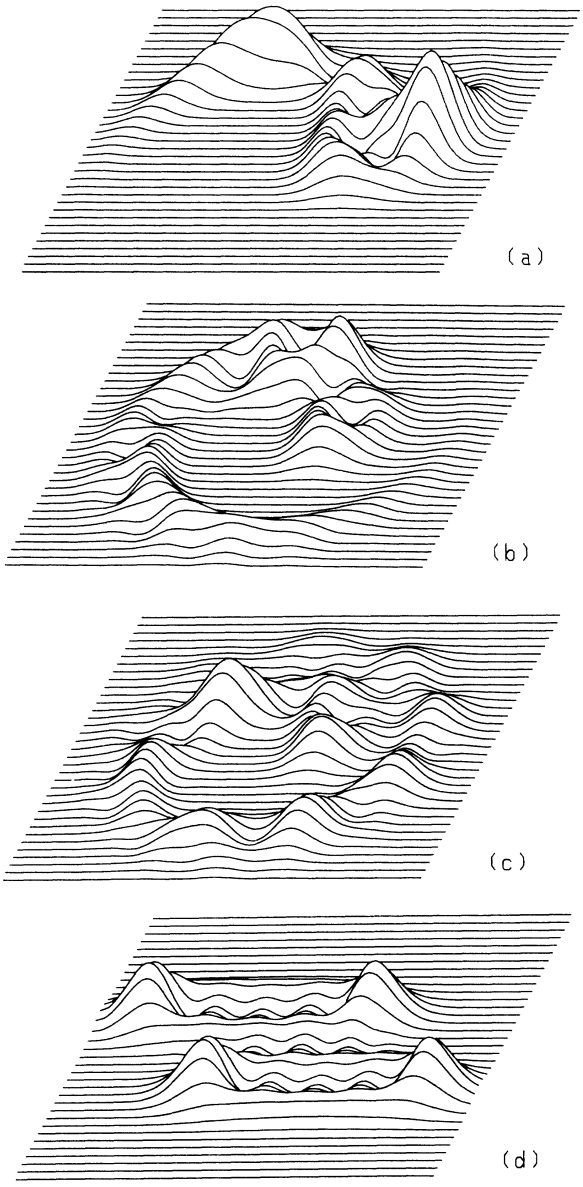

FIG. 5. Evolution of $\phi_{\mathcal{A}}$ as in Fig. 1. (a)–(c) have parameters $m=4$, $\alpha_0=2$, $\nu=1$, $d=7$, and $\gamma=0.05,0.15,0.25$. (d) belongs to $m=4$, $\alpha_0=2.5e^{i0.7}$, $\nu=0.8$, $d=7$, and $\gamma=\pi$.

There is also seen a small interference surf due to their proximity. This is some secondary effect of the interaction. In Fig. 5(d) the average intensity is again zero. This contrasts with the case from Fig. 4(e), where it was $\langle E \rangle\neq 0$. This suggests that there for the same revival (namely, $n=2$) a symmetry-breaking process appeared. It was active because there it held $\alpha_0=0$ and the two charts of $\phi_{\mathcal{A}}$ could not be placed in the plane α. Figure 5(d) is the first suggestion that this process does not come if the charts of $\phi_{\mathcal{A}}$ can be placed in the plane α. We expect that the equality $\langle E \rangle=0$ holds not only if $\gamma=2\pi/n$ (n natural) and if these charts could be placed in the plane α (this can be expected from the symmetry of $\phi_{\mathcal{A}}$). But we assume that $\langle E \rangle=0$, at least approximately, if γ changes between $2\pi/n$ and $2\pi/(n+1)$. It is clear that if the charts cannot be placed in the plane, new interferences change the picture and the equality $\langle E \rangle=0$ might be destroyed. This can be seen for a very small time of evolution of $\phi_{\mathcal{A}}$. Then it has nearly its starting form and it may certainly hold that $\langle E \rangle\neq 0$.

In Fig. 6 we demonstrate the evolution of $\phi_{\mathcal{A}}$ for displaced and fairly squeezed states with the parameters $m=1$, $|\alpha_0|=2$, $\nu=1$, $d=7$, $\varphi=1.57$ and $\gamma=0,0.25,0.75,2\pi/3$ for cases (a)–(d). We observe that one of the peaks rotates around the second one and finally it disappears. At an appropriate phase condition revivals reproduce it in a different number of equivalent replicas. This field is mixed from two components. The first one, which comes from the central peak, is phase independent and it corresponds to a vacuum state. The second one is composed of the three smaller peaks and it is therefore strongly phase dependent. We may say that the field is a superposition of a vacuum state and a "multiphase state," which is very similar to three coherent states shifted with $2\pi/3$.

In Fig. 7 we try to illustrate different phenomena. The parameters $m=4$, $\alpha_0=2$, $\nu=0.08$, $\gamma=\pi$, $d=6$ belong to case (a). We can see a double production of the starting Fock state, which has its boundary "exactly" above the coordinate center. Since both $\phi_{\mathcal{A}}$ for Fock states are too close, it holds again $\langle E \rangle\neq 0$. Case (b) corresponds to the parameters $m=1$, $\alpha_0=3$, $\nu=0.08$, $\gamma=\pi/2$, $d=5$. It shows the four time production of the first Fock state. This demonstrates the fact that revivals arise for an arbitrary shape of $\phi_{\mathcal{A}}$. Figure 7(c) has parameters $m=0$, $\alpha_0=2$, $\nu=2.5$, $\gamma=2\pi/3$, $d=6$. If $\phi_{\mathcal{A}}$ was large enough we might expect to obtain three strongly squeezed vacuum states. But we can see that these vacua are not "identical" because they overlap. From the above reasons it is again $\langle E \rangle\neq 0$. The final case corresponds to the parameters of Fig. 1(b), but for $\gamma=\pi+0.05$. It exhibits the fact that the start, from which we compute γ, can be chosen anywhere. Therefore the situation after the important angles $2\pi/k$ does not lead to a simple k-time production of the starting $\phi_{\mathcal{A}}$, but even the evolution, at least for short times, is identical to that at the beginning. The difference is that now k *identical* objects evolve in the same way. An exception from this arises if such patterns overlap [case (c)]. In Fig. 7(d) we observe the double reproduction of Fig. 1(b).

Finally Fig. 8 shows $\phi_{\mathcal{A}}$ with the parameters $m=0$, $\nu=0.08$, $\gamma=2\pi/12$, $d=7$ and $\alpha_0=2.5,3.5,4.5,5.5$ for the cases (a)–(d), respectively. We look at the transfer from a "classical" toward a "quantum" behavior of $\phi_{\mathcal{A}}$. For this specially chosen, the initial $\phi_{\mathcal{A}}$ reappears 12 times (if its "dimension" is sufficiently small) on the surrounding of the circle centered at $\alpha=0$ and having the radius of the middle shift $|\alpha_0|$ of $\phi_{\mathcal{A}}$. Ideas from the end of Sec. VI are demonstrated here. We can deduce that the critical radius for a coherent state and 12 revivals is $R_{\rm cr}=12R_{\rm coh}/\pi=5.5$, where $R_{\rm coh}$ is a fictitious radius of $\phi_{\mathcal{A}}^{\rm coh}$ for a coherent state. As a result $R_{\rm coh}=5.5\pi/12=1.44$, which is in good agreement with an approximate dimension of $\phi_{\mathcal{A}}^{\rm coh}$, calculated from $\phi_{\mathcal{A}}^{\rm coh}=e^{-|\alpha|2}/\pi$. For $R_{\rm coh}=1.44$ we obtain $\phi_{\mathcal{A}}^{\rm coh}(R_{\rm coh})\approx\phi_{\mathcal{A}}^{\rm coh}(0)/8$, so that neighboring $\phi_{\mathcal{A}}$ on the circle nearly

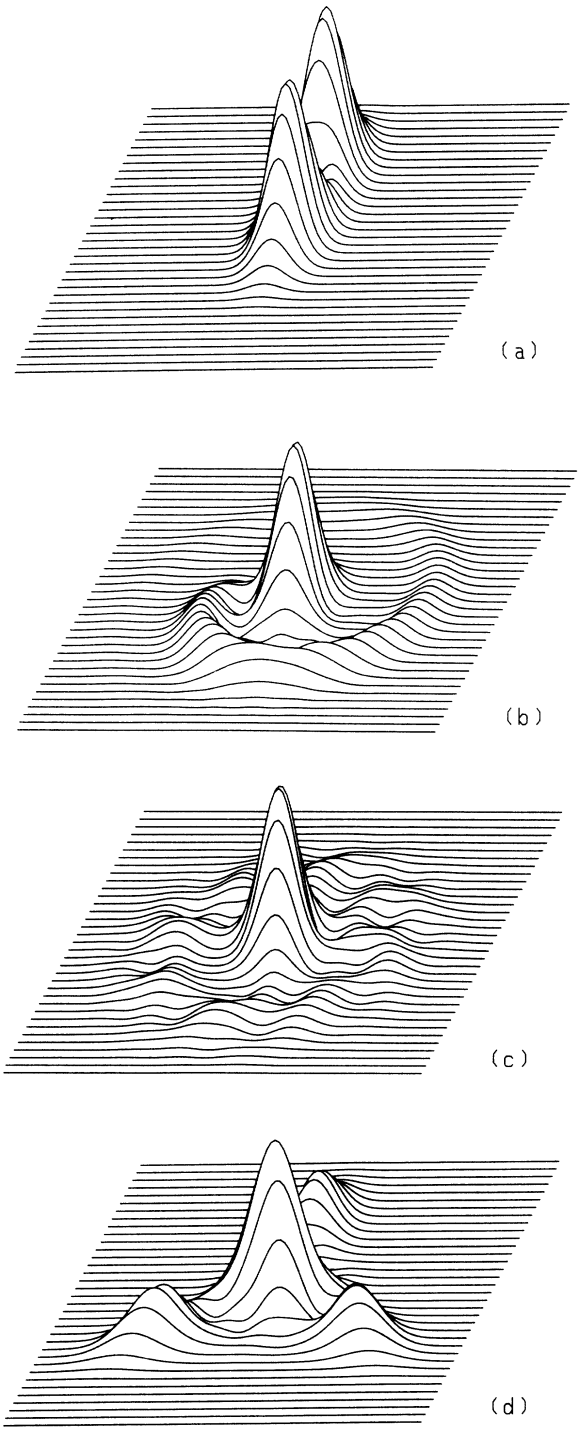

FIG. 6. The same as in Fig. 1 for the coefficients $m=1$, $\alpha_0=2e^{i1.5}$, $\nu=1$, and $d=7$. Surfaces (a)–(d) have $\gamma=0,0.25,0.75,2\pi/3$.

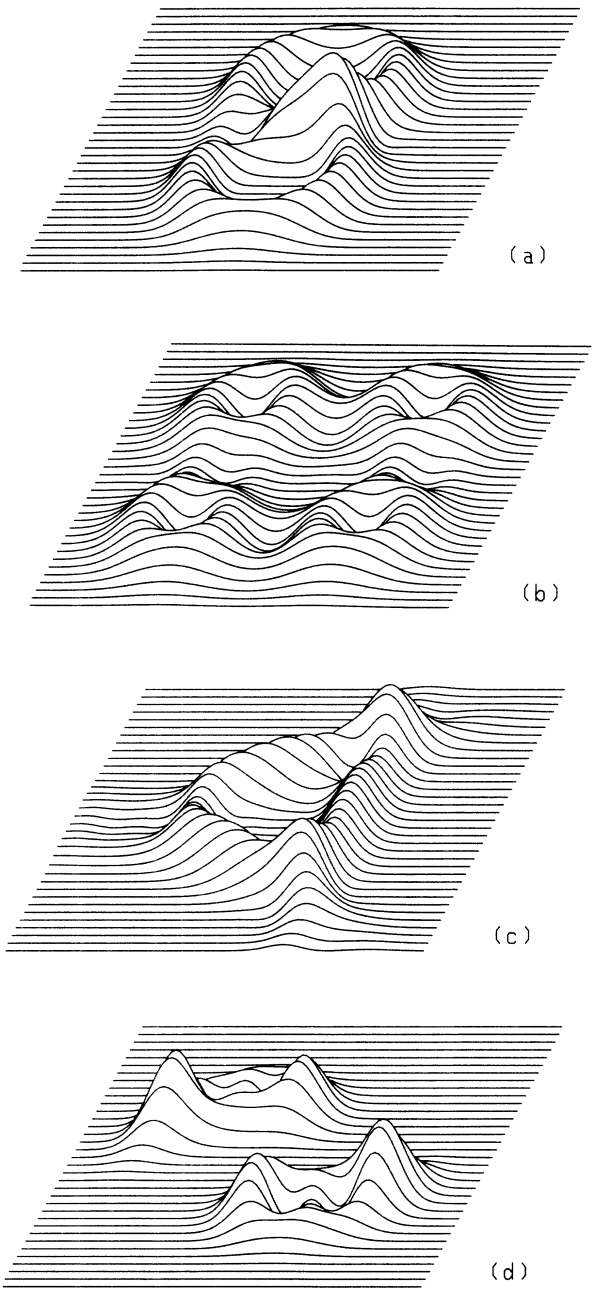

FIG. 7. As in Fig. 1, but every case (a)–(d) has its own parameters. They are $m=4$, $\alpha_0=2$, $\nu=0.08$, $\gamma=\pi$, $d=6$; $m=1$, $\alpha_0=3$, $\nu=0.08$, $\gamma=\pi/2$, $d=5$; $m=0$, $\alpha_0=2$, $\nu=2.5$, $\gamma=2\pi/3$, $d=6$; $m=2$ $\alpha_0=3.5$, $\nu=0.08$, $\gamma=\pi+0.05$, $d=7$ for (a)–(d).

do not overlap. We can also obtain the relation between α_0^{cr} and n, where α_0^{cr} is the critical shift of $\phi_{\mathcal{A}}^{coh}$, which we would like to observe placed n times on the circle with the radius $R_{cr}=|\alpha_0^{cr}|$. If we define R_{coh} by $\phi_{\mathcal{A}}^{coh}(R_{coh})=\phi_{\mathcal{A}}^{coh}(0)/10$ we easily obtain, putting $2n$ lines of length R_{coh} on the perimeter of the circle with R_{cr}, the relation

$$|\alpha_0^{cr}| \cong n/2 \ . \tag{7.1}$$

This relation introduces the minimal shift $|\alpha_0^{cr}|$, which must be chosen, if we want to gain quantum revivals of order n. For this order the parameter γ is $\gamma=2\pi/n=\pi/|\alpha_0^{cr}|$. Now we mention the fact, that for $\gamma=2\pi/k$, $|\alpha_0|>|\alpha_0^{cr}|$ and a coherent state as the input, we obtain a quite general field, which could be called a "multiphase coherent state." Such a field produces a quantum analogy of the classical intensity

$$E(r,t)=E_{clas}\mathrm{Re}\left\{\sum_{m=0}^{k-1}\exp\left[i\left[Kr-\omega t+\frac{2\pi m}{k}\right]\right]\right\}, \tag{7.2}$$

where K is the wave vector, r is the coordinate, and ω the frequency of the field. In the classical case all the moments of $E(r,t)$ are exactly zero. But for a quantum field prepared in MCS only the odd moments of E are zero. Since the intensity E concerns one mode, any measurement on the field destroys all components in the quantum analog of (7.2) simultaneously. The fact that for $k>0$ it holds $\langle E\rangle=0$, but $\langle E^2\rangle \approx E_{clas}^2$, suggests that the medium in which this field propagates should not have such a propensity for damage by high field intensities.

(ii) In classical physics the concept a phase of a monochromatic field is well based. This is not true in quantum mechanics. Many attempts have been made to invent a unitary phase operator with various levels of success. Here we introduce the concept of the antinormal phase distribution. Deeper theoretical investigation of the subject is out of our focus now.

Since the antinormal distribution $\phi_{\mathcal{A}}$ is normalized, we can introduce the antinormal phase distribution $\phi(\varphi)$ in the following way:

$$\phi(\varphi)=\int \phi_{\mathcal{A}}(r) r\, dr \ . \tag{7.3}$$

It is clear that this phase distribution is also normalized

$$\int \phi(\varphi) d\varphi = 1 \ . \tag{7.4}$$

$\phi(\varphi)$ for a coherent state could be easily found, so that we do not present it here. Intuitively it can be expected that it is formed by a peak at the point of the phase of the coherent shift β. It has good limit properties for large $|\beta|$. The field then becomes quasiclassical, the phase uncertainty disappears and $\phi(\varphi)$ approaches a δ function. The above definition of $\phi(\varphi)$ is one of many possible. It has certainly some disadvantage but it can present the field in some way. The normal phase distribution, defined analogously to the antinormal one, is singular and therefore does not show a phase uncertainty where it should be. The symmetric phase distribution loses its sense because it could be also negative.

In Figs. 9(a)–9(d) we show a representative example of phase distributions $\phi(\varphi)$ after (7.3) for $\phi_{\mathcal{A}}$ from Figs 8(a)–8(d). We can see in detail how the phase breaks down in many "channels" when the starting shift α_0 grows. For small shift α_0 no oscillations appear in $\phi(\varphi)$, which is rather blurred due to the presence of the Kerr interaction. The case (b) reveals first oscillations on a broad background. In cases (c) and (d) α_0 still grows, oscillations become deeper, and the flat background slowly disappears. For very large shifts we would practically see 12 δ functions placed at regular intervals. Figure 9 gives a detailed view of the evolution of the phase of $\phi_{\mathcal{A}}$. It

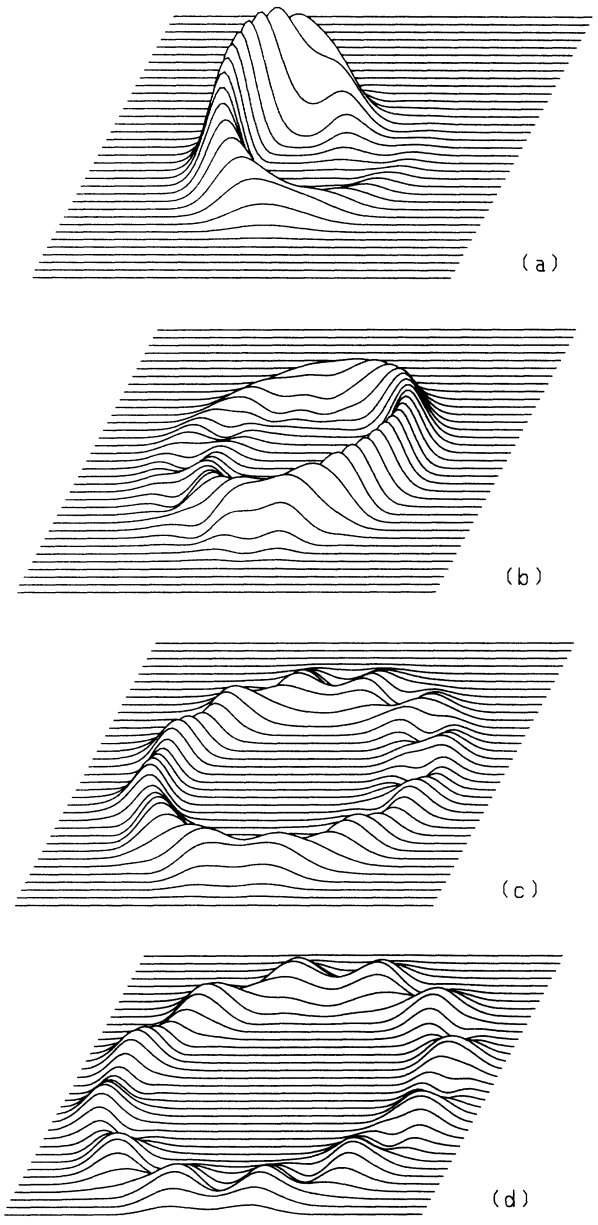

FIG. 8. Dependence of $\phi_{\mathcal{A}}$ on the parameter α_0. The surfaces (a)–(d) correspond to the constants $m=0$, $\nu=0.08$, $\gamma=2\pi/12$, $d=7$, and $\alpha_0=2.5, 3.5, 4.5, 5, 5$.

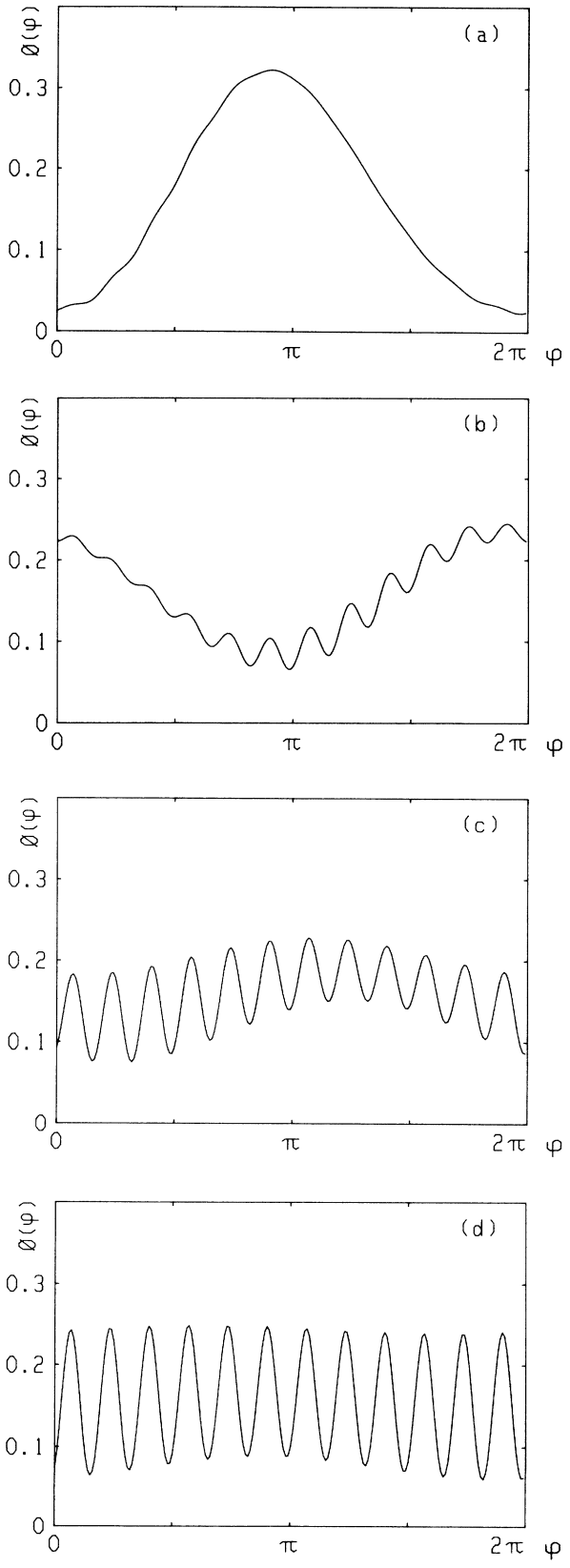

FIG. 9. Antinormal phase densities $\phi(\varphi)$ after the definition (7.3) for the fields from Fig. 8. The cases (a)–(d) from Fig. 8 correspond to (a)–(d) here. We can see the transfer toward the discrete values of a phase.

clearly illustrates how revivals influence the phase of a field. Notice that in all cases (a)–(d) oscillatory maxima and minima are at the same value of φ. This can be expected from our previous discussion.

(iii) Wave functions in (3.8) can give information about the production and motion of wave packets. They can be used for calculations of the coordinate moments $\langle q^n \rangle$. The probability density $|\langle q|U_3|\beta,m\rangle_g|^2$ serves as a weight in the integral

$$\langle q^n \rangle = \int q^n |\langle q|U_3|\beta,m\rangle_g|^2 dq \ .$$

We show a few examples of the probability density below. It would also be possible to find the moments of the intensity $\langle E^n \rangle$. To this goal it is necessary to calculate the moments $\langle p^n \rangle$ from the p representation of the state $U_3|\beta,m\rangle_g$. This way seems to be much easier than the direct differentiation of $C_{\mathcal{A}}$ in (4.1).

In Figs. 10(a) and 10(b) we present a dependence of $|\langle q|U_3|\beta,m\rangle_g|^2$ on q for the parameters and $\phi_{\mathcal{A}}$ from Figs. 3(a) and 3(b). The case (a) shows the wave function for a squeezed tenth Fock state. The wave function keeps its sharp form in Fig. 10(b), the sidepeaks move far from the center and they become broader. The rotation of $\phi_{\mathcal{A}}$ results in oscillation of the variations $\Delta^2 p$, $\Delta^2 q$, but it must hold that $\Delta^2 p \Delta^2 q \geq 2\pi$. If we found the p representation of the wave function, we would see that its shape becomes narrower during the evolution in Figs. 10(a) and 10(b). Since here it is $\langle p \rangle = \langle q \rangle = 0$, fluctuations of the variations $\Delta^2 p$, $\Delta^2 q$ represent a flow of energy in the field between its potential and kinetic form.

In Fig. 10(c) we show the same as in Figs. 10(a) and 10(b), but for parameters from Fig. 4(b). The evolution here is reminiscent of Fig. 10(b). Oscillations with variable period arise into the broad hill of the wave function here. The other three peaks experienced some change, too.

Figure 10(d) shows a continuation in the evolution of the wave function from Fig. 10(c). It corresponds to the parameters for $\phi_{\mathcal{A}}$ from Fig 4(e). The transfer of the shapes of the wave function is very interesting. Here it is very similar to the elongated form for the fourth Fock state, except for the asymmetry around the zero value of q. Physically the asymmetry means that the probability of finding any particle in the right side of the wave packet is higher than on the left side. It is evident now that $\langle E \rangle \neq 0$.

(iv) As the last example we exhibit some typical photon-number distributions $p(n)$ of the fields presented above. They are calculated similarly as in the numerical part of Ref. 1. First the matrix elements $\langle n|\beta,m\rangle_g$ are found, by the method shown there. Then we multiply each of these elements by the factor $\exp[i(\gamma/2)n(n-1)]$, resulting from U_3. Also we use the numbers $\langle n'|D(a_0)|n\rangle$ in the identity

$$\sum_n |n\rangle\langle n| = 1 \ ,$$

applied between the states $\langle n'|D(a_0),U_3|\beta,m\rangle_g$. The results are the matrix elements $\langle n'|D(a_0)U_3|\beta,m\rangle_g$. These are used to find the photon-number distributions.

In Fig. 11(a) are plotted the photon-number distribu-

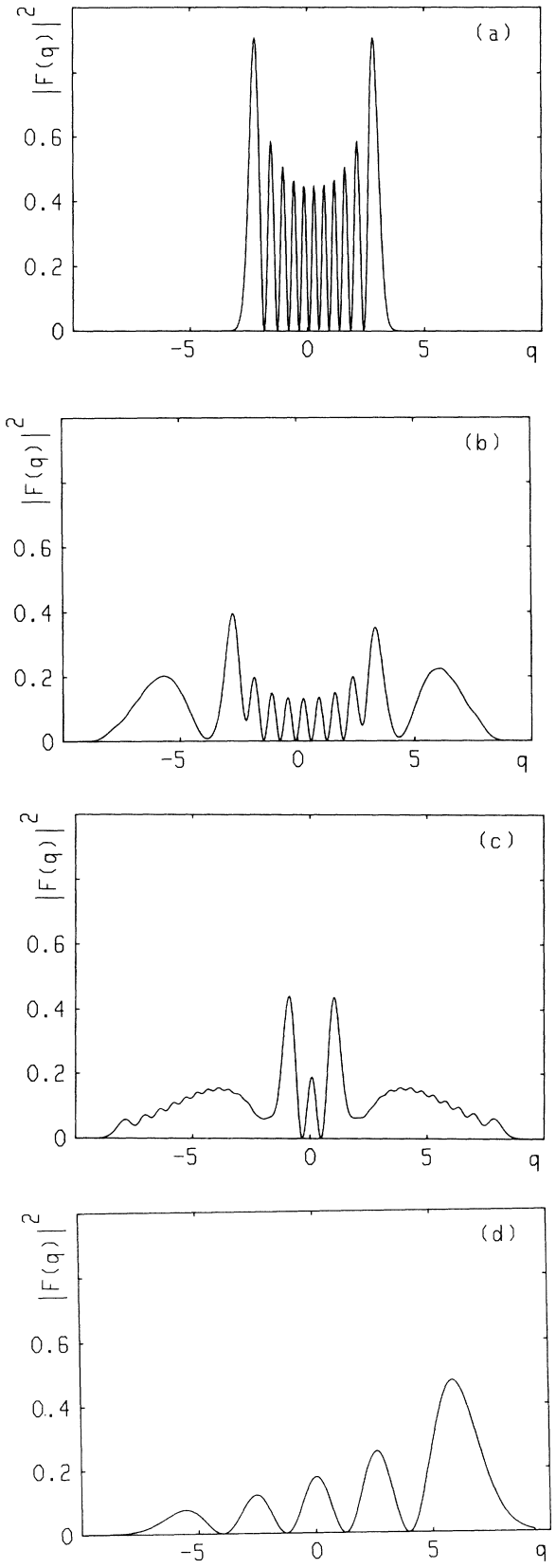

FIG. 10. Dependence of the probability density $|F(q)|^2=|\langle q|U_3|\beta,m\rangle_g|^2$ on q. Cases (a)–(d) correspond to the parameters in Figs. 3(a), 3(b), 4(b), and 4(e). A result of the "symmetry-breaking" process can be seen in (d).

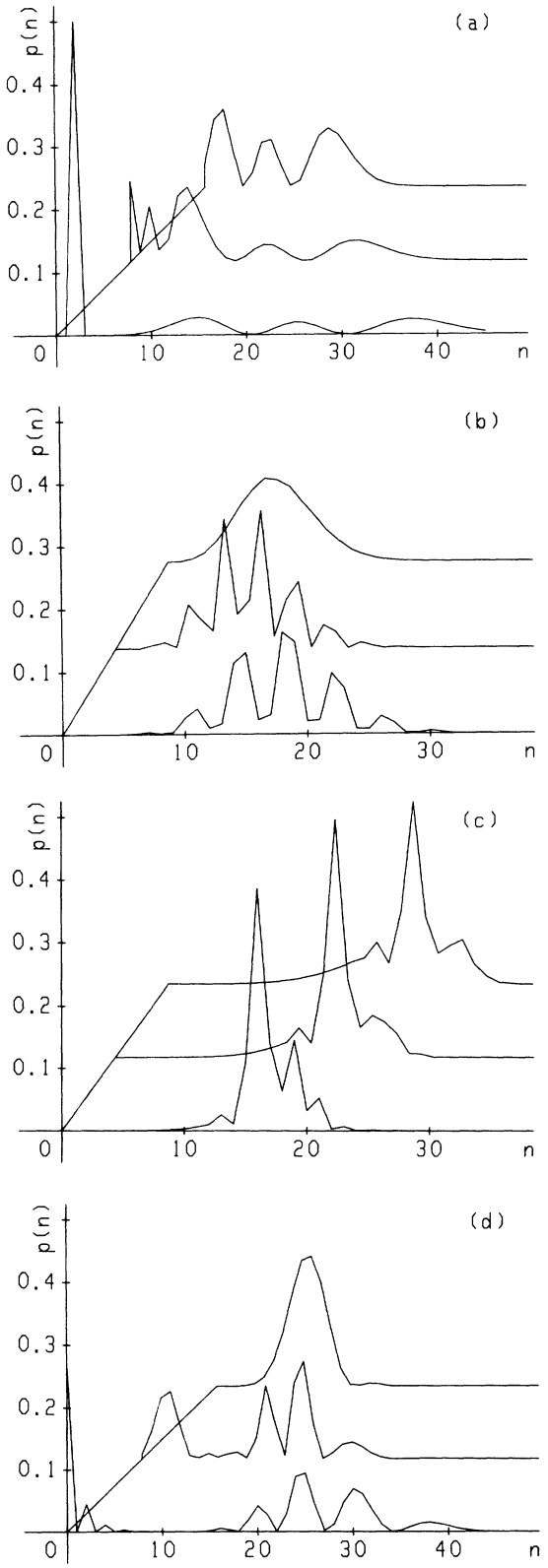

FIG. 11. Dependence of the photon-number distributions for $D(a_0)U_3|\beta,m\rangle_g$ on a_0. If the variable a_0 changes from the nearest curve toward the farthest one, the parameters for the cases (a)–(d) are $m=2$, $\alpha_0=2.5$, $\nu=0$, $\gamma=\pi$, $a_0=|a_0|e^{i\pi/2}$, $|a_0|=2.5,1.25,0$; $m=0$, $\alpha_0=3$, $\nu=0$, $\gamma=\pi$, $a_0=3,1.55,0$; $m=1$, $\alpha_0=4$, $\nu=0$, $\gamma=0.15$, $a_0=1e^{i(1.88+\varphi)}$, $\varphi=0,0.3,0.6$; $m=0$, $\alpha_0=3$, $\nu=0.7$, $\gamma=2\pi/3$, $a_0=3,1.5,0$.

tions for the states $D(a_0)U_3|\beta,m\rangle_g$ with parameters $m=2$, $\alpha_0=2.5$, $\nu=0$, $\gamma=\pi$, $a_0=|a_0|e^{i\pi/2}$. $|a_0|$ is 2.5, 1.25, 0, starting from the nearest curve. We can see $p(n)$ for $\phi_{\mathcal{A}}$ which is composed of two circles for Fock states lying on different parts of the point $\alpha=0$. The three curves correspond to three positions of the displaced coordinate center, as it moves from the center of one of the circles toward the point $\alpha=0$. The first curve is formed by a peak, corresponding to the circle having the coordinate center inside, and by a three-hill-like part for the displaced Fock state from the second circle. This means that there is the probability 0.5 to find one particle in the field and the same probability to find any other result, which lies dominantly between 10 and 40 particles. As the coordinate center goes toward the point $\alpha=0$, the peak diminishes and it would seem, from $p(n)$, that both circles join together, forming $p(n)$ of the starting $|\beta,m\rangle_g$ [U_3 itself does not change $p(n)$ statistics].

Figure 11(b) presents similar phenomenon in $\phi_{\mathcal{A}}$, but now the parameters are $m=0$, $\alpha_0=3$, $\nu=0$, $\gamma=\pi$ and $a_0=3,1.5,0$, beginning from the nearest curve. The coordinate center moves on the real axis $\mathrm{Im}\alpha=0$ between the two hills of $\phi_{\mathcal{A}}$, which correspond to two equivalent coherent states displaced to the points $\alpha=3e^{i\pi/2}$, $3e^{-i\pi/2}$. Interferences start to appear in $p(n)$ even for a small shift a_0. Successively they become broader, but do not disappear. Fields with "modulated Poissonian" statistics could be produced in this way.

Figure 11(c) demonstrates sub-Poissonian behavior in $p(n)$. The parameters are $m=1$, $\alpha_0=4$, $\nu=0$, $\gamma=0.15$, $a_0=1e^{i(1.88+\varphi)}$, where φ is 0,0.3,0.6, starting from the nearest curve. The coefficients are similar to those from Ref. 3, but now $m=1$. We observe that the middle curve is probably the most sub-Poissonian. Interferences and broadening destroy the other two peaks.

The last example in Fig. 11(d) returns to higher γ, where revivals of a small multiplicity appear in $\phi_{\mathcal{A}}$. The parameters are $m=10$, $\alpha_0=3$, $\nu=0.7$, $\gamma=2\pi/3$, $a_0=3,1.5,0$, beginning at the nearest curve. The squeezed vacuum, reproduced three times, is "observed" first from the center of one of the vacua, then from the middle point between $\alpha=0$ and the previous one, and finally from the point $\alpha=0$. In the first curve we can see typical two-photon oscillation from the squeezed vacuum having the coordinate center inside and slow interference oscillations from the two remaining vacua. This field, formed from a superposition of a squeezed vacuum and some coherent part, could have applications in atomic physics. We might expect that a stimulated scattering in the presence of this field will be of a combined type. This scattering will pass with some probability as in the presence of a squeezed vacuum and with another probability as in a coherent field. But the evolution will also be affected by some coherent effects from a simultaneous action of both parts. The curves continuously change toward the last one, which looks like it would correspond to a displaced and squeezed vacuum.

VIII. CONCLUSION

We have used displaced and squeezed Fock states, investigated in Refs. 1 and 2, as the input of the Kerr medium. The resulting states were presented by various examples of distributions. A special type of these states are the "multiphase coherent states" (see Fig. 8). We have found that they have important unclassical properties. These states could probably be observed by carefully performed experiments. In practice the field intensities are usually strong, therefore revivals of higher number seem to be observable. We presume that they will be masked by noise and their $\phi_{\mathcal{A}}$ will look like they have the form of a continuous circle. We think that the lowest revivals should be searched at first. It will probably be more difficult to produce the multiphase coherent states than the squeezed light. Their detections could be realized by photon-number measurements in the Kerr interferometer.[3] These measurements should be compared with the theoretical results for $p(n)$, examples of which are in Fig. 11. The MCS states can be especially characterized by their phase distributions. Figure 9 shows that MCS preserve their unclassical behavior in the limit of a strong field.

The $U_3|\beta,m\rangle_g$ states generalize both the crescent states from Ref. 3 and the displaced and squeezed Fock states from Ref. 1. They also form a special basis for calculation, similar to $|\beta,m\rangle_g$ states. Preparation of these states would be even more difficult than the production of MCS. But since the Fock states will probably be produced in the future, we may think of their application in the Kerr medium.

ACKNOWLEDGMENTS

The author would like to thank Dr. J. Peřina for his stimulating discussions and encouragement.

APPENDIX

We will exhibit the derivation of a Hermite polynomial, from its generating function, in the elements $\langle\alpha|\beta,m\rangle_g$ in (2.3). This way was used in nearly all formulas presented above.

In Ref. 1 we show that

$$\langle\alpha|S(\zeta)D(\beta)\exp(\lambda a^{\dagger})|0\rangle=\exp(\lambda^2 A+\lambda B)\langle\alpha|\beta\rangle_g\ , \tag{A1}$$

where A,B are defined below (2.3). We call the second expression in (A1) the generating function of $\langle\alpha|\beta,m\rangle_g$. From (A1), the definition of the Hermite polynomials

$$\mathrm{H}_n(z)=(-1)^n e^{z^2}\frac{d^n}{dz^n}e^{-z^2} \tag{A2}$$

and the substitution $z=-\sqrt{-A}\,(\lambda+B/2A)$ we obtain

$$\langle \alpha|\beta,m\rangle_g = \frac{1}{\sqrt{m!}}\frac{\partial^m}{\partial\lambda^m}\langle\alpha|S(\xi)D(\beta)\exp(\lambda a^\dagger)|0\rangle|_{\lambda=0}$$

$$= \langle\alpha|\beta\rangle_g \frac{1}{\sqrt{m!}}\exp(-B^2/4A)(-\sqrt{-A})^m \frac{d^m}{dz^m}\left|_{\lambda=0} e^{-z^2} = \frac{1}{\sqrt{m!}}\langle\alpha|\beta\rangle_g(\sqrt{-A})^m H_m(z)\right|_{\lambda=0}. \quad \text{(A3)}$$

This procedure can be easily generalized if more differentiations, analogous to that from (A3), must be performed.

[1] P. Král, J. Mod. Opt. **37**, 889 (1990).

[2] M. S. Kim, F. A. M. De Oliveira, and P. L. Knight, Opt. Commun. **72**, 99 (1989); the same subject has been presented in *Coherence and Quantum Optics 6*, edited by J. H. Eberly, L. Mandel, and E. Wolf (Plenum, New York, 1989); M. S. Kim, F. A. M. de Oliveira, and P. L. Knight, Phys. Rev. A **40**, 2494 (1989); F. A. M. de Oliveira, M. S. Kim, and P. L. Knight, *ibid.* **41**, 2645 (1990).

[3] M. Kitagava and Y. Yamamoto, Phys. Rev. A **34**, 3974 (1986).

[4] G. J. Milburn, Phys. Rev. A **33**, 674 (1985).

[5] D. J. Daniel and G. J. Milburn, Phys. Rev. A **39**, 4628 (1989).

[6] V. Peřinová and A. Lukš, J. Mod. Opt. **35**, 1513 (1988); V. Peřinová, A. Lukš, and M. Kárska, *ibid.* **37**, 1055 (1990); V. Peřinová and A. Lukš, Phys. Rev. A **41**, 414 (1990).

[7] J. Peřina, R. Horák, Z. Hradil, C. Sibilia, and M. Bertolotti, J. Mod. Opt. **36**, 578 (1989).

[8] R. P. Bishop and A. Vourdas, J. Phys. A **20**, 3743 (1987).

[9] H. P. Yuen, Phys. Rev. A **13**, 2226 (1976).

[10] J. Peřina, *Quantum Statistics of Linear and Nonlinear Optical Phenomena* (Reidel, Dordrecht, 1984); R. J. Glauger, *Quantum Optics*, edited by S. M. Kay and A. Maitland (Academic, London, 1970).

[11] V. Peřinová, Opt. Acta **28**, 747 (1981).

[12] W. H. Louisell, *Quantum Statistical Properties of Radiation* (Wiley, New York 1973).

[13] N. N. Lebedev, *Special Functions and their Applications* (Prentice-Hall, Englewood Cliffs, 1965).

[14] B. Yurke and D. Stoler, Phys. Rev. Lett. **57**, 13 (1986); Phys. Rev. A **35**, 4846 (1987); Physica B **151**, 298 (1988); and references therein.

[15] I. Sh. Averbukh and N. F. Perelman, Phys. Lett. A **139**, 449 (1989).